

Superconducting transport properties of grain boundaries in $\text{YBa}_2\text{Cu}_3\text{O}_7$ bicrystals

D. Dimos and P. Chaudhari

IBM Research Division, Thomas J. Watson Research Center, Yorktown Heights, New York 10598

J. Mannhart

IBM Research Division, Zürich Research Laboratory, CH-8803 Rüschlikon, Switzerland

(Received 11 August 1989)

Previous work on the superconducting transport properties of individual grain boundaries in thin-film bicrystals of $\text{YBa}_2\text{Cu}_3\text{O}_7$ has been extended to provide a more comprehensive picture of their weak-link characteristics. Grain boundaries with three different geometries have been studied; the transport properties of all three types of boundaries are essentially identical, which implies that the poor superconducting coupling between grains is a result of the intrinsic structural disorder at the boundary. The grain-boundary critical current densities in bicrystal films prepared by evaporation and postannealing and by laser ablation are also in good agreement; this result demonstrates that the transport properties are insensitive to preparation technique and, thus, are not dominated by the diffusion of substrate impurities into the boundary region. High grain-boundary resistivities and low $J_c R_n$ products imply that the boundaries act as strong barriers to current flow with locally depressed order parameters. Strong magnetic hysteresis, associated with trapped intragranular flux, is observed; this hysteretic behavior is also responsible for an increase in the grain boundary J_c for $H_{\text{app}} > 300\text{--}500$ Oe.

I. INTRODUCTION

Clearly the most disappointing characteristic of the high- T_c cuprate superconductors, from an applications viewpoint, is the low values of the transport critical current densities obtained with polycrystalline samples, especially in comparison to the very high values obtained for single-crystal films. By measuring the superconducting transport properties of individual grain boundaries and their adjacent grains in $\text{YBa}_2\text{Cu}_3\text{O}_7$ thin-film bicrystals, we initially provided direct evidence that grain boundaries are responsible for low critical current densities and the extreme sensitivity of J_c to small magnetic fields.¹ We were also able to demonstrate that the grain boundary J_c is quite sensitive to the misorientation angle, even when the Cu-O planes in the adjacent crystals are essentially parallel, which was expected to be the most favorable geometry for high critical currents.² These results strongly imply that poor superconducting coupling across grain boundaries is an intrinsic characteristic and, not surprisingly, efforts to achieve improved and reproducible processing and properties have yielded only modest increases in the critical densities of sintered materials.

While it has been firmly established that grain boundaries in $\text{YBa}_2\text{Cu}_3\text{O}_7$ are weak links (i.e., a region of weakened superconductivity), a number of important questions remain. The most crucial concerns the mechanism by which the order parameter, which is equivalent to the density of Cooper pairs or to the amplitude of the pair wave function, is suppressed or even reduced to zero at the grain boundary, since such understanding may suggest whether possible remedies exist. Furthermore, it is important to establish to what extent the low critical current densities of polycrystalline samples of

$\text{YBa}_2\text{Cu}_3\text{O}_7$ and of the other high- T_c superconductors are due to the intrinsic characteristics of grain boundaries and to what extent they are controlled by other factors. It is also interesting to compare the properties of the grain-boundary weak links to the properties of more standard weak links to test the applicability of theoretical descriptions and to assess the potential of these grain boundaries for device applications. We have tried to address some of these issues by extending our previous work on the properties of individual grain boundaries in $\text{YBa}_2\text{Cu}_3\text{O}_7$. In this report, we present a more extensive description of the grain-boundary I - V characteristics and of their transport behavior as a function of temperature and magnetic field than was previously provided. Important and new information about the relationship between the superconducting transport properties and the structural properties of grain boundaries, and the possible role of anisotropy, has been obtained by measuring the critical current density as a function of misorientation angle for three different grain-boundary geometries.

II. EXPERIMENTAL PROCEDURES

Thin-film bicrystals of $\text{YBa}_2\text{Cu}_3\text{O}_7$ were prepared by epitaxial growth using oriented bicrystals of SrTiO_3 as substrates.² The substrates were fabricated either by hot pressing two single crystals at 1450°C or by sintering a SrTiO_3 pellet containing two oriented seed crystals at 1650°C . In the latter case, the bicrystal forms by migration of the original boundaries of the seed crystals over a distance of a few hundred microns. The samples prepared using both types of substrates gave the same results.

Most of the films were prepared by simultaneous

electron-beam evaporation of the three metal species onto heated substrates ($\approx 400^\circ\text{C}$) in a background oxygen pressure of about $20\ \mu\text{torr}$. The films, which were amorphous as deposited, were subsequently crystallized by annealing at about 925°C and then oxygenated by slow cooling in flowing O_2 . The films grow with an epitaxial relationship to the substrate so that the crystallography prescribed by the substrate is reproduced in the film. An optical micrograph of the surface of a typical epitaxially grown bicrystal film is shown in Fig. 1. The grain boundary is clearly visible in the center of the picture. The surface is dotted with CuO precipitates: these precipitates are formed as excess Cu is rejected from the film during epitaxial growth. The precipitates are easily removed by lightly polishing the sample which shows that they are confined to the surface. The small rectangular regions which are present correspond to domains in which the c axis lies in the plane of the film. These domains are parallel to the in-plane $[100]$ directions so that the misorientation angle between the two single crystals is visible.

For comparison, a bicrystal film was also produced by a laser-ablation technique, as previously described.³ In this method, an excimer laser is used to ablate a sintered pellet of $\text{YBa}_2\text{Cu}_3\text{O}_7$ in an oxygen pressure of 0.2 torr. Epitaxial films are produced directly by deposition of the ablated material onto a heated substrate with a surface temperature of $650\text{--}700^\circ\text{C}$. The samples are then slow cooled in a 700-torr oxygen atmosphere to yield a well-oxygenated film.

For this study, bicrystals with three different grain-boundary geometries were fabricated, as illustrated in Fig. 2. In the $[001]$ tilt boundaries [Fig. 2(a)], the c axes are essentially perpendicular to the plane of the film so that the Cu-O planes in the adjacent grains are parallel. The angle θ between the principal in-plane directions defines the misorientation (tilt) angle. It should be noted

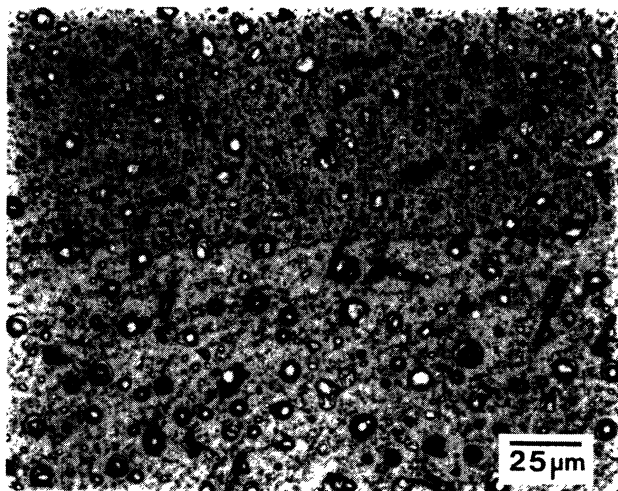


FIG. 1. Optical micrograph of the surface of a bicrystal film produced by evaporation and postannealing. The grain boundary runs through the center. Surface precipitates of CuO and small c -axis in-plane domains are visible. In this case, $\theta = 40^\circ$, as measured by x-ray diffraction.

that the films are twinned so that the a and b axes are macroscopically equivalent. In Fig 2(b), the c axes of the adjacent grains are misaligned by an angle ϕ in a plane normal to the grain-boundary plane; this misorientation produces a $[100]$ tilt boundary. In this case the principal in-plane directions, when projected onto the plane of the film, are aligned across the boundary. In Fig. 2(c), the misorientation angle γ between the c axes is in a plane parallel to the boundary plane. Here, the a (or b) axes are normal to the boundary plane so that a simple $[100]$ twist boundary is formed. The misorientation angles of the samples were determined to $\pm \frac{1}{2}^\circ$ using back reflection Laue x-ray diffraction. For all of the samples, the boundaries were roughly symmetric; however, alignment errors typically introduced some degree of asymmetry ($1^\circ\text{--}2^\circ$). For many samples, the misorientation is not fully described by just one of the simple geometries in Fig. 2; however, the misorientation of each sample can be completely specified by giving the angle for each component in Fig. 2, since these components are orthogonal.

The films, which were typically $0.5\ \mu\text{m}$ thick, were subsequently patterned with an excimer laser, as previously described.^{1,4} Narrow conducting lines (microbridges),

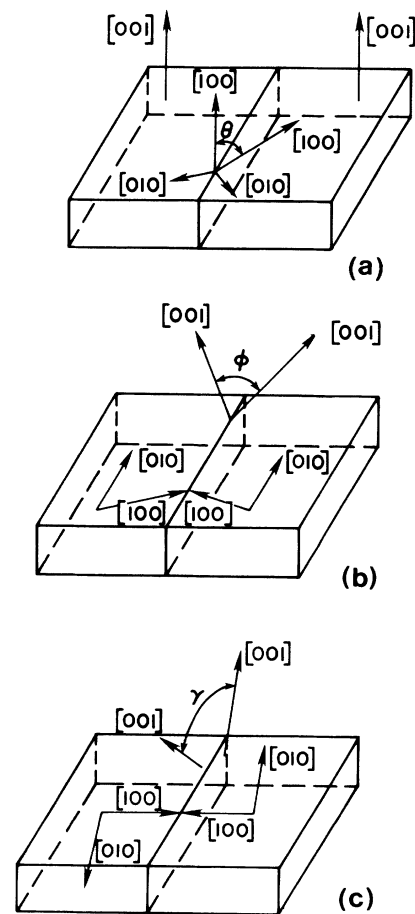


FIG. 2. Schematic diagram showing the important crystallography of the three grain boundaries geometries studied: (a) $[001]$ tilt boundary; (b) $[100]$ tilt boundary; and (c) $[100]$ twist boundary.

approximately 4–20 μm wide and 20–60 μm long, were formed within the two single grain regions and across the grain boundary. The microbridges were positioned to avoid large surface precipitates and domains with the c axis in the film plane. The current-voltage characteristics of each line were measured using a four-point technique. The critical current densities were determined by dividing the maximum zero-voltage current, using a 2- μV criterion, by the cross-sectional area of the patterned line. The electrical contacts to the film were made with aluminum wirebonds. In most cases, wirebonding directly to the film surface yielded contact resistances of sufficient quality ($\approx 20\text{--}50\ \Omega$) that ohmic heating at the wirebonds was insignificant. However, with the very high J_c films, evaporated Ag contacts were used to reduce the contact resistivities.

III. RESULTS

A. I - V Characteristics

Typical plots of voltage versus current density for single grain and single grain-boundary microbridges from the same sample (at 4.2 K) are shown in Fig. 3. The critical current density is quite well defined in both cases due to the sharpness of the transition. For this sample, the critical current density of the microbridge containing the grain boundary ($J_c = 2.6 \times 10^5\ \text{A/cm}^2$) is almost 2 orders of magnitude lower than the critical current density of the grain ($J_c = 1.6 \times 10^7\ \text{A/cm}^2$). Since it is always found that the grain boundary J_c is substantially less than for either adjacent grain ($J_c^{\text{gb}}/J_c^{\text{G}} < 0.1$), except for low-angle grain boundaries where the two values can be comparable, the reduction in J_c is attributed to the grain boundary, as previously demonstrated.^{1,2} Observations by low-temperature scanning electron microscopy (LTSEM)

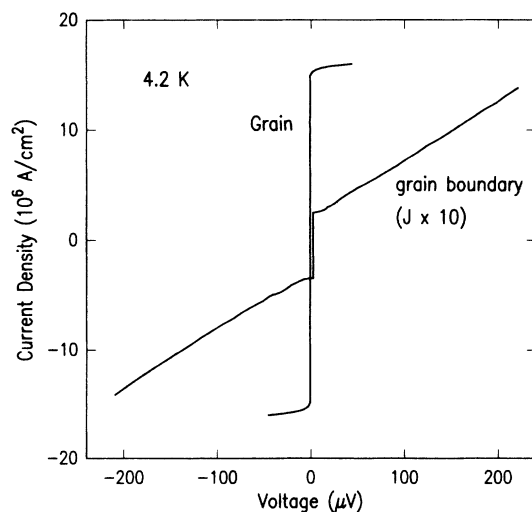


FIG. 3. Current density versus voltage for a single grain and single grain-boundary microbridge at 4.2 K. The current density values for the grain boundary curve have been multiplied by a factor of 10.

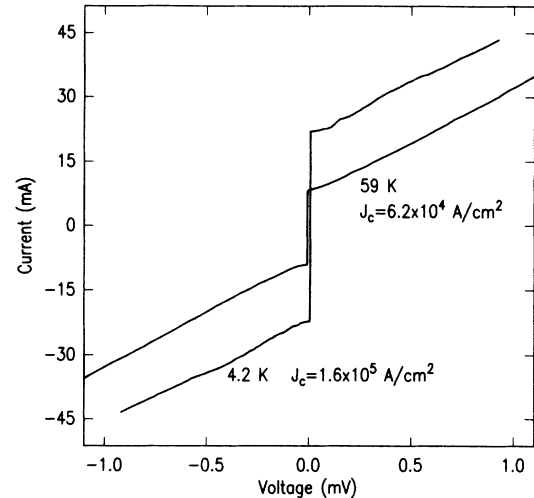


FIG. 4. I - V curves of a weak-link grain boundary at 4.2 and 59 K.

have provided additional confirmation that the voltage drop is confined to the vicinity of the grain boundary until the intragranular J_c is exceeded.⁵

For comparison, the I - V characteristics for two other single grain boundaries are shown in Figs. 4 and 5. For all grain boundaries, the transition from zero to finite voltage is abrupt, especially at low temperatures. In addition, this transition is sometimes hysteretic, as illustrated in Fig. 5. For currents in excess of I_c , the normal-state resistance R_n of most grain boundaries is relatively constant up to a few millivolts (Figs. 3 and 4). In one sample, this behavior was observed up to 75 mV. However, other grain boundaries display a clear increase in the dynamic resistance with increasing voltage over a similar voltage range, as illustrated in Fig. 5. This behavior cannot be accounted for only by local heating, since it persists up to T_c , where lower current levels reduce heat-

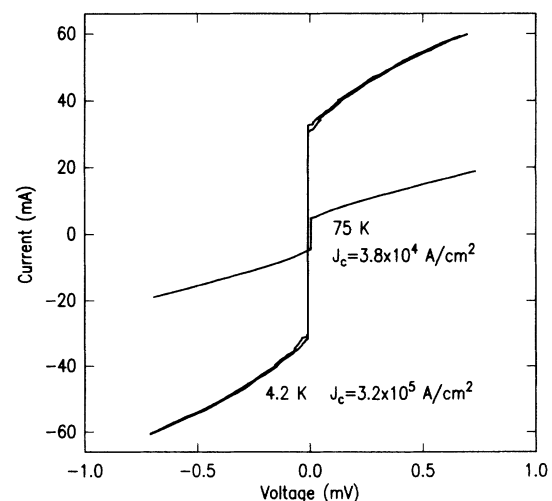


FIG. 5. I - V curves of a weak-link grain boundary at 4.2 and 75 K.

ing effects. For the former type of samples, (i.e., those with $R_n \approx \text{const}$), the grain-boundary resistance is roughly independent of temperature (compare the 4.2- and 59-K characteristics in Fig. 4) up to the transition temperature. A noticeable decrease in resistance with increasing voltage, as seen in the negative voltage branch of the grain-boundary curve in Fig. 3 and in the positive voltage branch of the 59-K curve in Fig. 4, is also commonly observed in the I - V characteristics of these boundaries.

The grain boundary I - V characteristics are often asymmetric about the origin in both the zero-voltage and resistive regions. For example, Fig. 3 shows a case where there is about a 30% difference in I_c for current flow in the two directions. Warming the sample above T_c and recooling typically modifies the degree of asymmetry without changing the total zero-voltage current range. (Consequently, I_c has been taken as half of the sum of I_c in both directions.) Warming and recooling was also found to affect the position of the low-voltage bumps in the I - V curves;⁶ these features, which were previously reported,⁷ are clearly visible in the 4.2-K characteristics in Fig. 4. LTSEM observations of the spatial variation of the grain-boundary resistance suggest that the structure in the I - V curves are self-excited resonances which are very sensitive to the presence of trapped flux in the boundary or nearby in the grains.⁵ The critical current asymmetry is also probably due to the presence of trapped flux. An additional asymmetry in the I - V curves is illustrated in both Figs. 3 and 4. Here, the positive voltage branch in Fig. 3 and the negative branch at 59 K in Fig. 4 are quite linear, except very near $V=0$, while the resistance is clearly decreasing over the entire range in the opposing branches.

For the samples in which R_n is roughly constant, the $I_c R_n$ products have been calculated. Table I lists the values of J_c , the normal-state resistivity ρ_n , and $I_c R_n$ ($\equiv J_c \rho_n$) for these boundaries at 4.2 K. While there is a difference of almost 2 orders of magnitude between the lowest and highest $I_c R_n$ values obtained for samples with similar critical current densities, the value for most samples is between about 1 and 4 mV. The highest $I_c R_n$ values were obtained from the laser-ablated film. However, there is no obvious relationship between the grain boundary J_c and the $I_c R_n$ product. The value of 0.06 mV, which seems abnormally low, was obtained for

TABLE I. The values of J_c , the normal-state resistivity ρ_n , and $J_c R_n$ ($\equiv J_c \rho_n$) for the grain boundaries at 4.2 K.

J_c (A/cm ²)	ρ_n ($\Omega \mu\text{m}^2$)	$I_c R_n$ (mV)
1.1×10^4	5.9	0.65
2.5×10^4	7.65	1.9
5.0×10^4	1.7	0.85
7.9×10^4	3.0	3.75
1.0×10^5	1.37	1.4
1.6×10^5	0.75	1.2
3.0×10^5	0.26	0.8
3.2×10^5	0.02	0.06
4.1×10^5	0.84	3.4
4.7×10^5	0.77	5.4

a sample that has the highest intragranular J_c and the sharpest transition for any of the evaporated films. Since the critical current density of this grain boundary is typical for good samples, the low $I_c R_n$ product is not necessarily a pathological value.

In contrast to the grain boundaries, the I - V characteristics of the grains exhibit a smooth voltage onset followed by a rapid increase in voltage with increasing current. As a result, I - V curves could only be obtained within a narrow voltage range without excessive heating. In addition, the intragranular I - V characteristics are completely symmetric about the origin.

B. Magnetic field effects

As previously shown, the grain boundary critical current density is extremely sensitive to small applied magnetic field.^{1,7} This behavior is illustrated in Fig. 6, which is a series of current-voltage curves at 4.2 K for different applied field strengths. While the grain boundary J_c is suppressed in a relatively monotonic fashion with increasing field strength up to about 300–400 Oe, clearly, the largest incremental suppression of the critical current density occurs for small applied fields. For this sample, the grain boundary J_c at an applied field of only 70 Oe is reduced from its zero-field value by about a factor of 20. This degree of suppression is typical for the bicrystals and is consistent with the field dependence of J_c commonly observed in bulk polycrystalline samples.^{8,9} In contrast, the critical current density of the grains is in-

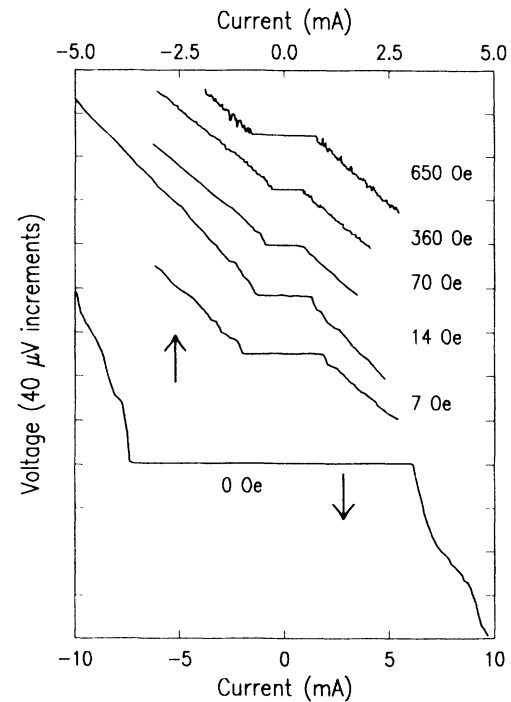


FIG. 6. I - V curves for a grain boundary at 4.2 K as a function of applied field strength. The field is applied perpendicular to the plane of the film and, thus, parallel to the grain-boundary plane. The current axes for the zero-field curve and the $H > 0$ curves are at the bottom and top, respectively.

dependent of applied field up to ≈ 300 Oe. This comparison demonstrates that the magnetic field penetrates preferentially at the grain boundary and, thus, verifies that the grain boundary is a region of weakened superconductivity.

While no distinct secondary maxima have been observed in plots of J_c^{gb} versus H for small applied fields, the grain boundary J_c exhibits an increase for field strengths in excess of 300–500 Oe (at 4.2 K). This increase in J_c^{gb} , which is seen in Fig. 6 for $H = 650$ Oe, is always accompanied by a significant increase in noise on the resistive branches of the I - V curves. Further increases in applied field, up to 1000 Oe, lead to little additional suppression of the boundary J_c . Often, a noticeable increase in the voltage noise is also observed at somewhat lower field strengths (e.g., 360 Oe in Fig. 6) where no increase in J_c occurs. At higher temperatures, these effects are observed at lower fields. For example, a similar increase in J_c and voltage noise was seen at 40 K with the same sample (as in Fig. 6) with a field of only 150 Oe.

The grain-boundary critical current density is also strongly dependent on the magnetic field history, which gives rise to strong hysteretic effects. Such hysteretic behavior is illustrated in Fig. 7, which shows two plots of the field dependence of J_c^{gb} determined by sweeping the field in the indicated directions after first adjusting the field to its maximum value. For this type of measurement, the critical current density peak is always found at a nonzero field value which is in the same sense as the starting field; this behavior differs from the initial zero-field-cooled curve, where the J_c peak is at $H_{app} = 0$. When the initial field strengths for the two sweeps have approximately the same absolute values, as in Fig. 7, the peaks are displaced almost symmetrically about $H = 0$. This type of hysteresis has also been found in polycrystalline samples.^{10,11}

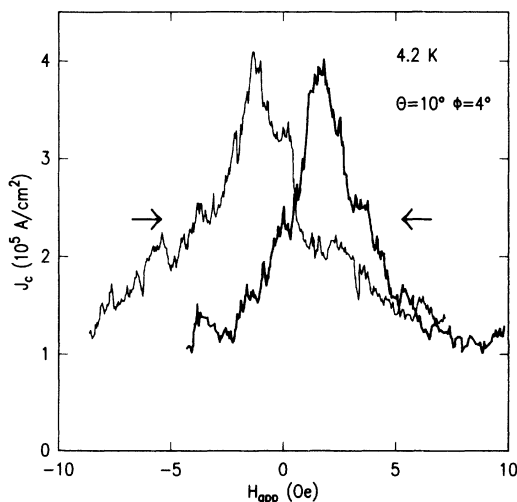


FIG. 7. Grain boundary critical current density as a function of applied field for field sweeps in opposing directions. The sweep is from positive to negative values for the bolder line.

C. Temperature dependence

In Fig. 8, the critical current density is plotted as a function of temperature for the two grains and their common grain boundary in a typical bicrystal sample. To directly compare the temperature dependencies, the critical current density for each set of data, is normalized with respect to the value at 5 K; however, the grain boundary J_c is about a factor of 10 less than for either grain. As pointed out previously, there are systematic differences between the temperature dependencies for the grains and the grain boundaries.⁷ In particular, the grain boundary J_c always exhibits a weaker temperature dependence at low temperatures (below ≈ 30 K) and a stronger temperature dependence at intermediate temperatures (between ≈ 30 and 70 K) than do the single grains. Still, the ratio of J_c^{gb}/J_c^G remains within about 10% of the value at 4.2 K, except very close to T_c . Near T_c , both the grain and grain-boundary critical current densities display a power-law dependence, such that $J_c \propto (1 - T/T_c)^p$. The power-law exponent for different samples varied from 1.6 to 2.7, with an average value of about 2; furthermore, the value of p for the grains and grain boundary for any particular sample were roughly the same. It should, however, be noted that the observed characteristics near T_c may be strongly influenced by the presence of spatial inhomogeneities, as observed by LTSEM.⁵

D. Orientation dependence

The relationship between the superconducting transport properties and the structural properties of the grain boundaries was explored by measuring the critical current density as a function of misorientation angle for the three grain-boundary geometries illustrated in Fig. 2.

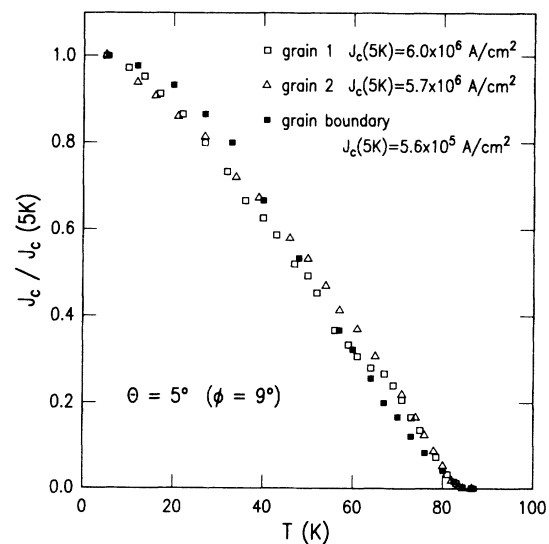


FIG. 8. Critical current density as a function of temperature for both grains and the grain boundary of one sample. The J_c values have been normalized to their values at 5 K, which are given in the figure.

The ratio of the grain boundary J_c to the average value for the two grains in a series of (evaporated) bicrystals is plotted as a function of the [001] tilt angle in Fig. 9. The ratio of critical current densities is used to emphasize the role of the grain boundary in limiting transport critical currents and to allow samples of different quality to be compared directly. The measured critical current density ratio is plotted on a logarithmic scale showing that the grain boundary J_c decreases very rapidly with increasing misorientation angle until a saturation value of about $\frac{1}{50}$ is reached for $\theta > 15^\circ - 20^\circ$. For low-angle boundaries ($\theta < 5^\circ$) the critical current densities were only slightly less than the grains and were independent of small applied fields, this behavior and the I - V characteristics were similar to that exhibited by the single grains. The transition from strong coupling for low-angle boundaries to weak-link behavior occurs over an angular range of $\theta = 5^\circ - 10^\circ$. The square data points are for samples where the out-of-plane misorientation angle ϕ is comparable to, or larger than, the in-plane value. The two points at $\theta = 5^\circ$, which are for samples with $\phi = 0^\circ$ (circle) and $\phi = 9^\circ$ (square), exhibit qualitatively different behavior. While the former exhibits little depression of J_c and no low-field sensitivity, the latter behaves as a weak link with a J_c ratio of about 1:10. This comparison illustrates the importance of additional degrees of misorientation.

In Fig. 10, the dependence of J_c^{gb}/J_c^G on the [100] tilt angle is plotted. The three different symbols are used to distinguish between samples that have an additional degree of in-plane misorientation ([001] tilt component) of 0° , 3° , and 5° . For the samples with $\theta = 5^\circ$, there is a clear transition from strong coupling, for $\phi = 0^\circ$, to weak-link behavior, for $\phi \geq 9^\circ$. The J_c ratio, the magnetic field dependence, and the I - V characteristics of these

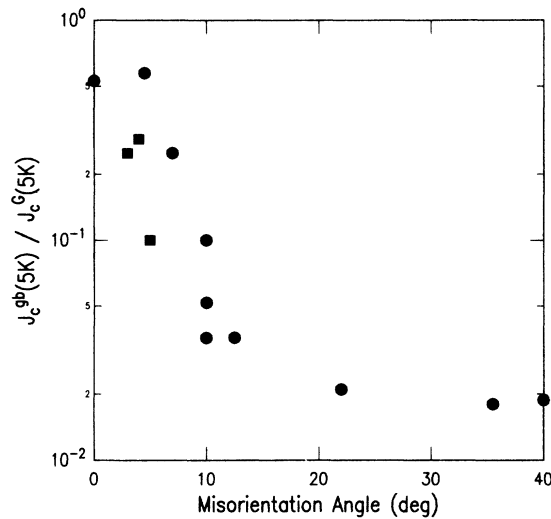


FIG. 9. Ratio of the grain-boundary critical current density to the average value of the critical current density in the two adjacent grains as a function of the misorientation angle in the basal plane. It should be noted that 45° is the largest misorientation angle, even in this orthorhombic crystal, due to fine-scale twinning on (110) planes.

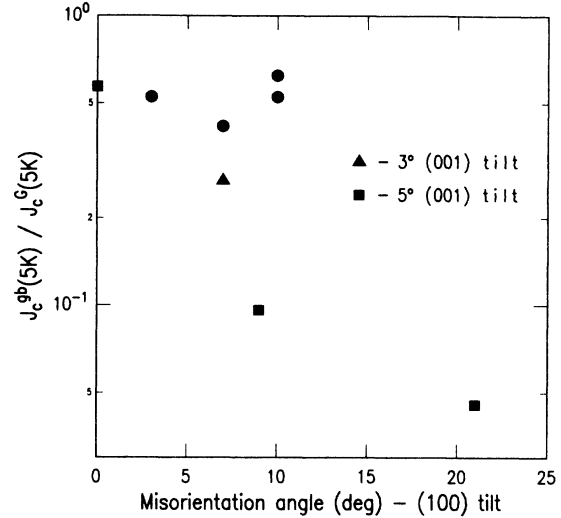


FIG. 10. Critical current density ratio as a function of the [100] tilt component.

high-angle boundaries are essentially the same as for the boundaries with large [001] tilt misorientations. However, for the samples with no additional in-plane misorientation, the boundary does not behave as a weak link up to 10° , in contrast to the behavior of the [001] boundaries; this result indicates that the grain-boundary characteristics are somewhat dependent on the specific grain-boundary geometry. The lack of data for large angles reflects the fact that good epitaxial growth becomes increasingly difficult as the angle between the film normal and the c axis increases.

The data from Figs. 9 and 10 has been incorporated with the data for the twist misorientations in Fig. 11. In this plot the total misorientation angle, as calculated

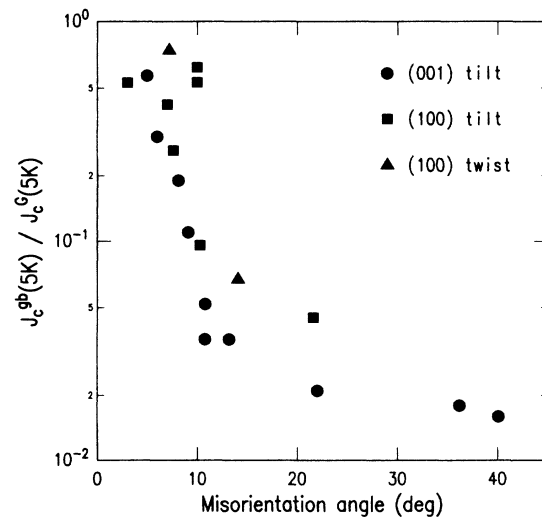


FIG. 11. Critical current density ratio as a function of the total misorientation angle. The different symbols distinguish the primary component of the misorientation with respect to the simple geometries in Fig. 1.

from the complete rotation matrix,¹² has been used. However, essentially all of the bicrystals can be considered to be primarily of one of the three simple geometries in Fig. 2. The different symbols are used to distinguish samples which are primarily of each different type. For all three grain-boundary geometries, there is a transition from strong coupling to weak coupling for angles larger than about 10° . For similar misorientation angles, the critical current density ratio is similar for all types. This type of master plot emphasizes the similarity in the properties of all the boundary geometries.

The data for the orientation dependence is summarized in Table II, which lists the critical current densities determined for both grains and the grain boundary for each bicrystal at 4.2 K. The three orthogonal components of the misorientation angle, as illustrated in Fig. 2, are given for each sample. In most cases the critical current densities for the two grains are almost identical; this indicates that properties of the film are spatially uniform even for the poor (low J_c) samples. In a few cases, J_c^{gb} has been measured at more than one microbridge along the boundary; the agreement between these values is also indicative of good uniformity. For the relatively high-angle boundaries exhibiting large depressions in J_c with a strong field dependence, the grain-boundary critical current densities (in the best samples) exceeded 10^5 A/cm² at 4.2 K and 10^4 A/cm² at 77 K. The grain boundary with $\theta=24^\circ$, which was prepared by laser ablation, was also a weak link. In this case, the grain-boundary critical current density was similar to the critical current density of other (good) high-angle boundaries, even though the

intragranular J_c at 4.2 K, which was in excess of 25×10^6 A/cm², was much larger than for any of the evaporated films. This result suggests that the absolute value of the critical current density of the weak-link grain boundaries is the fundamental quantity that characterizes the coupling strength at the grain boundary, and that the typical reduction factor of ~ 50 for the evaporated films is not necessarily an intrinsically significant quantity. This conclusion is satisfying since there is no reason that the critical current densities of the grains and the grain boundaries should be proportional.

IV. DISCUSSION

The large and systematic drop in J_c^{gb} with increasing misorientation angle, illustrated in Figs. 9–11 implies that J_c can be correlated to an intrinsic characteristic of the grain boundary. This drop in J_c can be due to local variations in structure and/or composition or to problems in coupling anisotropic superconductors of different orientations. In the latter case, the properties associated with the grain boundary should be relatively insensitive to the exact structural features of the boundary, but should depend strongly on the type of misorientation. For example, if the pair wave function was highly localized in the Cu-O planes or along the Cu-O-Cu bond directions, strong coupling between grains would occur only when the Cu-O planes were parallel (i.e., for [001] tilt boundaries) or when the Cu-O-Cu bonds remained aligned across the boundary (i.e., for [100] twist boundaries), respectively. However, the strong similarity in I - V characteristics, temperature and magnetic field

TABLE II. Orientation dependence of J_c (A/cm²) at 4.2 K.

θ	ϕ	γ	Grain 1	Grain 2	Grain Boundary
0	3	0	7.1×10^6	8.0×10^6	4.0×10^6
5	0	0	6.1×10^6	7.1×10^6	3.8×10^6
0	7	0	5.2×10^6	6.2×10^6	2.4×10^6
4	4	2	2.7×10^5	2.2×10^5	7.3×10^4
1.5	0	7	2.3×10^6	1.4×10^6	1.2×10^6
					1.7×10^6
3	7	0	5.9×10^6	5.3×10^6	1.5×10^6
7	4	0	1.4×10^5	1.8×10^5	4.0×10^4
0	10	0	1.9×10^6	2.2×10^6	1.3×10^6
0	10	0	4.4×10^6		2.8×10^6
5	9	0	6.0×10^6	5.7×10^6	5.6×10^5
9	1	0	7.2×10^6	3.6×10^6	5.8×10^5
10	4	0	7.8×10^6	8.0×10^6	4.1×10^5
10	4	0	7.0×10^6	6.1×10^6	2.4×10^5
13	2	0	3.8×10^6	3.4×10^6	1.6×10^5
1	1	14	5.8×10^6	3.6×10^6	3.0×10^5
22	0	2	8.0×10^5	2.6×10^5	1.1×10^4
24	0	1 ^a	$> 25.0 \times 10^6$ ^b		7.9×10^4
					1.7×10^5
					4.7×10^5
5	21	0	2.7×10^6	1.2×10^6	8.7×10^4
36	4	1	1.4×10^6	1.4×10^6	2.6×10^5
40	2	0	16.0×10^6		2.6×10^5

^aLaser-ablated film.

^b J_c (20 K) = 25×10^6 .

dependence, and suppression of J_c with misorientation angle between boundaries with very different geometries, suggests that the weak-link behavior is not caused by an anisotropic order parameter or an anisotropic effective mass.¹³

The superconducting order parameter can be strongly suppressed in the vicinity of a structural defect, such as a grain boundary, if the effective width of the defect ω is comparable to the coherence length ξ . The structural disorder at a grain boundary occurs as a natural consequence of the need to accommodate the lattice mismatch at the boundary plane. The structural features of grain boundaries can be described using either a polyhedral packing model or a simple dislocation model for low-angle boundaries, where the spacing d between parallel dislocations is given by $d = b/\theta$, in which θ is the misorientation angle and b is the Burgers vector of the dislocations. The [001] tilt boundaries are composed of edge dislocations with $b \approx 3.9 \text{ \AA}$; these dislocations are perpendicular to the film as previously observed by transmission electron microscopy.² The [100] tilt boundaries will be composed of edge dislocations that have the same Burgers vector but lie parallel to the plane of the film. The [100] twist boundaries should be composed of two sets of screw dislocations which form a square array. The two sets have $b \approx 3.9 \text{ \AA}$ and 11.7 \AA ; however, the latter can dissociate into three partials with $b \approx 3.9 \text{ \AA}$.¹⁴ With increasing misorientation angle, the dislocation spacing decreases until eventually the dislocation cores would begin to overlap. It should be noted that for a dislocation core radius of $r_0 \approx b$, the overlap condition of $d \approx 2r_0$ would occur at $\theta \approx 20^\circ$, which corresponds roughly to the angle for which J_c^{gb}/J_c^G reaches its minimum value. Although high-angle boundaries ($\theta > 15^\circ - 20^\circ$) can, thus, no longer be described as simple dislocation arrays, they can be viewed, to a first approximation, as a plane with a fairly uniform degree of structural disorder.

The effective width of a grain boundary is a quantity that is difficult to define precisely; however, diffraction experiments on a variety of materials and calculations based on simple elasticity theory both provide estimates for the lateral extent of the displacement field associated with the grain boundary.¹⁵ For high-angle boundaries, which were always found to act as weak links, it is estimated that the lattice distortions are essentially confined to within 1–2 lattice spacings on each side of the boundary plane. Consequently, the structural width for high-angle [001] and [100] tilt boundaries in $\text{YBa}_2\text{Cu}_3\text{O}_7$ is estimated to be $\approx 10 - 15 \text{ \AA}$. The structural width of [100] twist boundaries should be similar, even though the periodicity is partially determined by the c -axis spacing, since the unit cell in this direction can be split into three similar structural subunits with a size of $\approx 3.9 \text{ \AA}$.

Although in conventional superconductors ξ is generally at least an order of magnitude larger than typical lattice dimensions, this situation is not necessarily true in the high- T_c materials. While well-accepted values for the coherence lengths of the cuprate superconductors are generally lacking, it is known that the coherence lengths

for these materials are very short and highly anisotropic. Recent measurements of H_{c2} for $\text{YBa}_2\text{Cu}_3\text{O}_7$, which do not appear to be complicated by typical problems due to flux motion, yield values for the coherence length parallel to and perpendicular to the copper-oxygen planes of 16 and 3 \AA , respectively.¹⁶ Since this rather small value of the in-plane coherence length is comparable to the estimated width of the grain boundary, a strong local depression of the order parameter can occur over the length scale that characterizes a grain boundary. However, the mechanism by which the structural disorder locally suppresses or destroys superconductivity remains unclear. The local depression in the order parameter may be enhanced since the coherence length in the vicinity of the boundary can be smaller than its bulk value due to strong quasiparticle scattering at the boundary.¹⁷ This reduction in ξ would be consistent with the estimate by Deutscher,¹⁸ based on our measurements of the temperature dependence of the grain boundary J_c , that the effective in-plane coherence length at the boundary is about 4 \AA ($\equiv a_0$). Due to the anisotropy in ξ , the depression of Δ and, thus, the reduction of J_c should be most severe when the grain boundary plane is normal to the [001] direction, but this conclusion has yet to be directly tested.

While high-angle boundaries always act as weak links, strong coupling is maintained for low-angle boundaries, where the misorientation angle is less than about 5° . This latter result is not surprising since low-angle boundaries are composed of discrete dislocations separated by regions with relatively perfect lattice matching, where no depression of Δ is expected. While the dislocation density increases smoothly with increasing misorientation angle ($d \propto 1/\theta$), it is unclear whether the grain boundary J_c is related in a simple way to the dislocation density. In fact, it appears (Fig. 11) that there may be a fairly abrupt transition from strong-coupling to weak-link behavior when the misorientation angle exceeds some critical value. The situation for low-angle boundaries can be complicated, since the structural variations in the plane of the boundary associated with the individual dislocations will give rise to variations in the value of Δ along the plane of the boundary. Furthermore, the elastic stress field associated with the boundary becomes wider as the dislocation density decreases, since cancellation of the long-range stress fields associated with the individual dislocations becomes less effective as their spacing increases. However, these long-range elastic strains are probably less important than the large degree of disorder that occurs at the dislocation cores.

In addition to the intrinsic structural disorder, chemical segregation or deviations from the bulk stoichiometry in the vicinity of the grain boundary would be expected to lead to an additional reduction in the local condensation energy. Since appreciable interdiffusion can occur between the components of the films and the substrates during the high-temperature anneal, it was important to assess the possible contribution from such an additional effect. As reported previously,² no substantial enhancements in the concentrations of Sr or Ti were observed in the vicinity of a high-angle grain boundary, except very

near the film-substrate interface, from secondary-ion mass-spectrometry (SIMS) analysis using the field-imaging mode. Both this result and the observation that the critical current densities were not especially sensitive to extended diffusion anneals² implied that the grain boundary critical current densities were not strongly affected by interactions with the substrate. To further test this conclusion, a thin-film bicrystal was prepared by laser ablation. In this case, the maximum annealing temperature of 650°–700°C was about 250°C lower than the annealing temperature for the evaporated films. At this temperature, very little interdiffusion is expected. The agreement between the grain boundary J_c for the laser-ablated film and the other high-angle boundaries demonstrates that the critical current densities for the grain boundaries are not very sensitive to the preparation technique and, thus, are not dominated by the presence of substrate impurities at the boundary. However, these observations do not rule out the possibility that intrinsic deviations in stoichiometry occur at grain boundaries in $\text{YBa}_2\text{Cu}_3\text{O}_7$, as suggested by several authors.^{19–22}

A. Characteristics of grain-boundary weak links

While a depressed order parameter at the grain boundary reduces the depairing current across the boundary as compared to its bulk value, it is not clear that J_c^{gb} is actually determined by the coupling energy across the grain boundary. Alternatively, J_c^{gb} may be reduced to lower values by weak flux pinning along the boundary, since a local reduction in Δ also reduces the available pinning potential.²³ This situation can occur if the weak link is long enough to accommodate vortices.²⁴ The critical length, for an ideal rectangular geometry, is given by $L/\xi(T) \approx 3.5$,²⁵ where L is the length of the weak link and the width, $W \gg \xi(T)$. Since L must be on the order of $\xi(T)$ for the boundary to behave as a weak link, this latter possibility cannot be ruled out. The distinction between these descriptions is important because in the weak flux pinning picture the grain boundary J_c could be increased by introducing defects at the grain boundary, such as precipitates, which might act as pinning sites.

Evidence that the grain boundaries act as Josephson junctions, where $I_c = (2e/\hbar)E_j$, and not just as weak flux pinning channels, is provided by the observation of current steps in the I - V characteristics of a single grain boundary under microwave irradiation.²⁶ By examining the step heights as a function of microwave power, the current-phase relationship was found to be single valued although somewhat nonsinusoidal. This result is in agreement with similar measurements made on multigrain microbridges.²⁷ Although it is also possible to obtain current steps through the coherent motion of Abrikosov vortices, in practice this situation is difficult to achieve, since small inhomogeneities, which are likely in these samples, would lead to some pinning effects and, thus, reduce the coherency.²⁴

It is, therefore, interesting to ask if a definitive conclusion can be made about whether the grain-boundary weak links are tunnel junctions (SIS) or not (SNS , $SS'S$). As we previously discussed,⁷ a satisfactory fit to the tem-

perature dependence of the grain boundary J_c (Fig. 8) can be obtained using either the Ambegaokar-Baratoff equation for tunnel junctions by using a reduced energy gap [$\Delta(0) \approx 5$ meV] or with a model for SNS junctions due to Likharev.²⁴ Deutscher has shown that the power-law dependence near T_c can also be obtained with the Ambegaokar-Baratoff expression by recognizing that a considerable depression of the order parameter occurs at the interface between an insulator and a superconductor with a short coherence length and that this depression is strongest near T_c .¹⁸ Gross has recently pointed out that this behavior is similar to the situation which occurs at an S - N interface and that this similarity obscures the typical distinction between SIS - and SNS -type behavior.²⁸ Consequently, the temperature dependence of the critical current for both an SNS and an SIS (in the limit of a very short coherence length) junction is expected to be quite similar, especially near T_c , where $I_c \propto (1 - T/T_c)^2$. The near- T_c power-law exponents observed for the single grain-boundary samples are in reasonable agreement with this prediction.

A strong, local depression in the order parameter would also obscure any clear gap features in the I - V characteristics and, indeed, no features that can be clearly associated with the gap were found for any of the grain boundaries, even up to 75 mV. In addition, the low values for the $I_c R_n$ products are in agreement with the concept of a highly depressed order parameter in the vicinity of the grain boundary. An effective grain-boundary resistivity can be calculated from the measured normal-state resistance. For an estimated boundary width of about 10 Å, $\rho_{\text{gb}} \sim 0.1 \Omega \text{ cm}$ for the high-quality bicrystal samples. This rather high value is about 3 orders of magnitude larger than the resistivity of the single crystal regions of these films at T_c and suggests that the boundaries act as very strong scattering centers.

B. Magnetic field effects

While the J_c^{gb} versus applied field curves exhibit no distinct secondary maxima, as would be expected for an ideal, uniform Josephson junction, the observed behavior (Figs. 6 and 5 in Ref. 7) is similar to that found for some large Josephson junctions.²⁹ For our samples, the width of the junction is given by the width of the patterned line, which was typically 5–15 μm (10 μm for the sample of Fig. 7). The Josephson penetration depth is given by $\lambda_j = (\hbar/4\pi e \mu_0 J_c d)^{1/2}$, where d is taken to be about $2\lambda_0 \approx 3000$ Å. Since λ_j is 2–4 μm for J_c^{gb} between 1×10^5 and 4×10^5 A/cm² (Fig. 7), respectively, the high- J_c grain boundaries are all large junctions at low temperatures (i.e., $\lambda_j < W$). In large junctions, the $J_c(H)$ pattern is distorted by the self-field of the Josephson current and can become quite irregular in inhomogeneous junctions. However, ideal small-junction behavior was never observed, even at elevated temperatures, where $\lambda_j > W$. For grain boundaries with $J_c(4.2 \text{ K}) \ll 1 \times 10^5$ A/cm², the films had nonuniform microstructures, which gave rise to very complicated diffraction patterns.^{1,6} It should also be noted that the diffraction patterns obtained from the laser-ablated film were similar to the complicated pat-

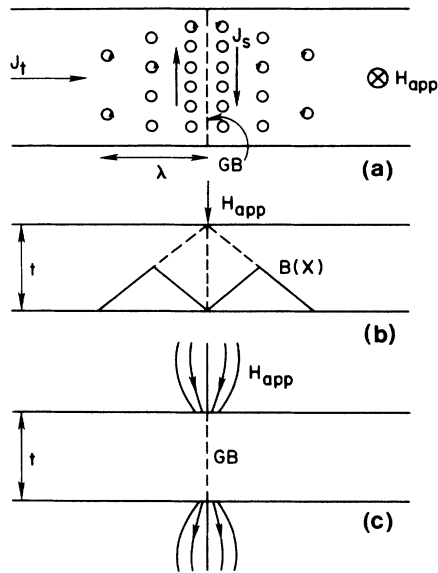


FIG. 12. (a) Schematic view (normal to the film) of the flux gradient and shielding currents established near the boundary with increasing field. The small circles are fluxons. The applied field, which is normal to the film, and the transport current J_t are shown. (b) Schematic cross-sectional view of the critical-state flux profile, which is established in the vicinity of the boundary with increasing (dashed) and decreasing (solid) field. (c) Schematic cross-sectional view showing how the magnetic flux is concentrated at the grain boundary. This strong concentration is released when flux penetrates through the bulk of the film.

terns seen in the nonuniform, low- J_c evaporated films.

The hysteresis due to magnetic fields (Fig. 7) can be attributed to the influence of the intragranular flux profile in the vicinity of the grain boundary as discussed by McHenry *et al.*¹¹ and Campbell.³⁰ As the magnetic field is increased from a zero-field-cooled condition, flux penetrates into the grains from the grain boundary. The critical-state flux gradient that is established gives rise to circulating shielding currents (J_s), as illustrated in Fig. 12(a). The presence of these circulating currents is equivalent to having an additional phase gradient along the boundary which adds to the phase gradient produced by the applied field. When the field is decreased, some of the flux is pushed out of the grains. The remaining intragranular flux, which is trapped, establishes a new critical-state flux gradient [Fig. 12(b)], in which the circulating currents and the resultant phase gradient near the boundary is reversed. When the phase gradient due to the trapped flux cancels that due to the applied field, the boundary critical current reaches a maximum; the J_c maximum will, thus, occur at an applied field greater than zero. This effect will be symmetric about $H_{app}=0$ for field sweeps in opposing directions, as observed. Similar hysteresis effects have been observed in NbN junctions, where the bulk electrodes also exhibit strong flux pinning.³¹

Although penetration of the field into the grains is expected once the field exceeds H_{c1} , hysteresis effects asso-

ciated with trapped intragranular flux are observed for very small applied fields (≈ 1 Oe). While the maximum effective field at the edge of the microbridge is larger than the applied field by roughly the width to thickness ratio of the microbridge (typically ~ 10), noticeable hysteresis is observed for fields substantially less than H_{c1} . However, even for $H < H_{c1}$, flux can still penetrate in from the boundary up to a distance of λ . The flux trapped in this region is presumably responsible for the low-field hysteresis. The increase in J_c^{gb} for fields strengths in excess of 300–500 Oe can also be attributed to a change in the intragranular flux profile near the boundary. As illustrated in Fig. 12(c), the field is strongly concentrated around the grain boundary for $H_{app} < H_{c1}$. Although some flux can penetrate into the film when $H_{app} > H_{c1}$, the field remains concentrated at the boundary until approximately H_m , which is the field at which the minimum magnetization is obtained in an M - H loop. In this field range, the magnetic flux strongly penetrates into the bulk of the film which reduces the flux concentration near the boundary. This is equivalent to locally reducing the applied field at the boundary, which causes a reversal of the phase gradient due to the intragranular flux profile; as before, this reversal leads to an increase in J_c . The noise in the resistive branches of the I - V curves for these larger applied fields, which is very erratic, is presumably due to intragranular flux motion in the vicinity of the boundary.

C. Bulk critical currents

According to these results, the critical current densities of untextured polycrystalline samples of $\text{YBa}_2\text{Cu}_3\text{O}_7$ will be controlled by the low and highly field-dependent critical current densities of high-angle grain boundaries. This conclusion remains valid even for highly textured microstructures in which the c axes of the grains are aligned, since this type of texturing does not eliminate high-angle [001] tilt boundaries. Nevertheless, it should be possible to obtain critical current densities in textured samples that are similar to the values for the high-angle [001] tilt boundaries^{32,33} which exceeded 10^5 A/cm² at 4.2 K and 10^4 A/cm² at 77 K for the good quality films (i.e., those with $J_c^G > 10^6$ A/cm²). These values are consistent with those obtained for laser-ablated polycrystalline films on MgO substrates in which the c axes are perpendicular to the film but the a and b axes are unaligned.³⁴ Critical current densities in this range, which might be quite acceptable for some applications, have also been achieved by producing highly textured microstructures in bulk samples.^{35,9} These values should also be relatively insensitive to small misalignments of the c axes according to the behavior observed for low-angle [100] tilt and [100] twist boundaries. However, the presence of high-angle [001] tilt boundaries will still cause the bulk critical current density to be strongly suppressed by small magnetic fields. In fact, even for $H_{app}=0$, the bulk J_c may be severely limited by the magnetic field produced by the sample current (self-field); this effect will be especially important for large samples. For untextured materials, critical current densities are expected to be lower due to the

abundance of grain boundaries which are parallel to the basal planes. However, the critical current densities of most polycrystalline samples prepared to date are almost certainly limited by a combination of intrinsic and extrinsic factors, examples of the latter being microcracking and the presence of second phases.³⁶ To make materials with critical current densities that approach single-crystal values and which do not exhibit a weak-link field dependence, a high degree of alignment both normal to and within the basal plane must be achieved; this is an unprecedented requirement for processing of a polycrystalline material.

While the experiments on $\text{YBa}_2\text{Cu}_3\text{O}_7$ bicrystals have directly verified that grain boundaries in this system are weak links, there is a variety of evidence that suggests that this behavior is generic to all of the cuprate superconductors. Specifically, the critical current densities of polycrystalline samples of La-Sr(Ba)-Cu-O, Bi-Sr-Ca-Cu-O, and Tl-Ba-Ca-Cu-O compounds are typically both low and highly field dependent.³⁷⁻⁴¹ In addition, measurements of the complex ac susceptibility in bismuth and thallium cuprates display loss peaks associated with weak intergrain coupling that are similar to those observed for polycrystalline $\text{YBa}_2\text{Cu}_3\text{O}_7$.^{42,43} If the intergranular weak-link behavior exhibited by the cuprate superconductors is simply due to structural features of the grain boundaries, and is not related to the mechanism for superconductivity in these materials, then other superconductors with short coherence lengths should behave similarly. An especially interesting case for comparison are the Chevrel phase superconductors, typified by PbMo_6S_8 , which has a coherence length and lattice parameter of 25 and 10 Å, respectively.⁴⁴ However, even with a coherence length that approaches the lattice dimensions, the properties of polycrystalline PbMo_6S_8 appear quite similar to those of more conventional superconductors.⁴⁵ For example, reasonably high critical current densities ($> 10^4$ A/cm² at 14 T and 4.2 K) with conventional field dependencies have been obtained. In addition, an inverse relationship between critical current density and grain size has been reported, which suggests that grain boundaries act primarily as flux pinning centers. Another interesting case for comparison is $(\text{Nd}_{1-x}\text{Ce}_x)_2\text{CuO}_4$ for which

$\xi_{\parallel} \simeq 70 \text{ \AA}$.⁴⁶ Since grain boundaries, in which the Cu-O planes are parallel, should not behave as weak links in this compound if it is only the relative magnitude of ξ and the width of the grain boundary that is important, the properties of this material should provide important clues about the mechanism for producing grain-boundary weak links.

V. CONCLUSIONS

All grain boundaries in $\text{YBa}_2\text{Cu}_3\text{O}_7$, except for very low-angle ones, are Josephson junctions, which are responsible for the relatively low and highly magnetic-field-dependent critical current densities of polycrystalline materials. The similarities in the transport characteristics of grain boundaries with very different geometries and the relative insensitivity of these characteristics to preparation conditions imply that this weak-link behavior is an intrinsic property of these grain boundaries. While the mechanism for the depression of Δ at the grain boundary remains unclear, a strong local depression of the order parameter can be expected since the length scale that characterizes the extent of disorder at the boundary is comparable to the coherence length. Since short coherence lengths are a common feature of the high- T_c superconductors, it is not surprising that grain boundaries in this entire class of materials seem to act as weak links. The inherent weak-link characteristics of grain boundaries will make it difficult to process high- T_c compounds for large scale applications that require very high critical current densities; however, these same properties may turn into an advantage for potential device applications, such as superconducting quantum interference devices.

ACKNOWLEDGMENTS

The authors would like to thank G. Koren and A. Gupta for preparing the laser-ablated bicrystal film. We would like to acknowledge R. Gross, S. J. Kaplan, D. R. Clarke, C. C. Tsuei, T. M. Shaw, J. Chi, Y. Yeshurun, and T. K. Worthington for stimulating discussions and useful comments.

- ¹P. Chaudhari, J. Mannhart, D. Dimos, C. C. Tsuei, J. Chi, M. M. Oprysko, and M. Scheuermann, *Phys. Rev. Lett.* **60**, 1653 (1988).
- ²D. Dimos, P. Chaudhari, J. Mannhart, and F. K. LeGoues, *Phys. Rev. Lett.* **61**, 1653 (1988).
- ³G. Koren, A. Gupta, E. A. Giess, A. Segmüller, and R. B. Laibowitz, *Appl. Phys. Lett.* **54**, 1054 (1989).
- ⁴J. Mannhart, M. Scheuermann, C. C. Tsuei, M. M. Oprysko, C. C. Chi, C. P. Umbach, R. Koch, and C. Miller, *Appl. Phys. Lett.* **52**, 1271 (1988).
- ⁵J. Mannhart, R. Gross, K. Hipler, R. P. Huebener, C. C. Tsuei, D. Dimos, and P. Chaudhari, *Science* **245**, 839 (1989).
- ⁶P. Chaudhari, D. Dimos, and J. Mannhart, *IBM J. Res. Develop.* **33**, 299 (1989).
- ⁷J. Mannhart, P. Chaudhari, D. Dimos, C. C. Tsuei, and T. R.

McGuire, *Phys. Rev. Lett.* **61**, 2476 (1988).

- ⁸S. Jin, R. A. Fastnacht, T. H. Tiefel, and R. C. Sherwood, *Phys. Rev. B* **37**, 5828 (1988).
- ⁹N. McN. Alford, J. D. Birchall, W. J. Clegg, and K. Kendall, *J. Appl. Phys.* **65**, 2856 (1989).
- ¹⁰J. E. Evetts and B. A. Glowacki, *Cryogenics* **28**, 641 (1988).
- ¹¹M. E. McHenry, M. P. Maley, and J. O. Willis, *Phys. Rev. B* **40**, 2666 (1989).
- ¹²The total misorientation angle is given by $\cos^{-1}[(t-1)/2]$, where t is the trace of the rotation matrix, which is given by $t = \cos\theta \cos\phi + \cos\theta \cos\gamma + \cos\phi \cos\gamma + \sin\theta \sin\phi \sin\gamma$.
- ¹³V. G. Kogan, *Phys. Rev. Lett.* **62** 3001 (1989).
- ¹⁴M. F. Chisholm and D. A. Smith, *Philos. Mag. A* **59**, 181 (1989).
- ¹⁵C. B. Carter and S. L. Sass, *J. Am. Ceram. Soc.* **64**, 335 (1981).

- ¹⁶U. Welp, W. K. Kwok, G. W. Crabtree, K. G. Vandervoort, and J. Z. Liu, *Phys. Rev. Lett.* **62**, 1908 (1989).
- ¹⁷E. V. Thuneberg, J. Kurkijärvi, and D. Rainer, *Phys. Rev. B* **29**, 3913 (1984).
- ¹⁸G. Deutscher, *IBM J. Res. Develop.* **33**, 293 (1989).
- ¹⁹D. M. Kroeger, A. Choudhury, J. Brynestad, R. K. Williams, R. A. Padgett, and W. A. Coghlan, *J. Appl. Phys.* **64**, 331 (1988).
- ²⁰S. E. Babcock, T. F. Kelly, P. J. Lee, J. M. Seuntjens, L. A. Lavanier, and D. C. Larbalestier, *Physica* **152C**, 25 (1988).
- ²¹Y.-M. Chiang, J. A. S. Ikeda, and A. Roshko, in *Ceramic Superconductors II, Research Update 1988*, edited by M. F. Yan (American Ceramic Society, Westerville, Ohio, 1988), pp. 607–618.
- ²²S. E. Babcock and D. C. Larbalestier, *J. Appl. Phys.* **55**, 393 (1989).
- ²³D. P. Hampshire, X. Cai, J. Seuntjens, and D. C. Larbalestier, *Supercond. Sci. Technol.* **1**, 12 (1988).
- ²⁴K. K. Likharev, *Rev. Mod. Phys.* **51**, 101 (1979).
- ²⁵M. Y. Kuprianov, K. K. Likharev, and L. A. Maslova, in *Proceedings of the 14th International Conference on Low Temperature Physics*, edited by M. Krusius and M. Vuorio (North-Holland, Amsterdam, 1975), Vol. 4, p. 104.
- ²⁶R. Gross, S. J. Kaplan, J. Chi, and D. Dimos (unpublished).
- ²⁷B. Hauser, B. B. G. Klopman, G. J. Gerritsma, J. Gao, and H. Rogalla, *Appl. Phys. Lett.* **54**, 1368 (1989).
- ²⁸R. Gross (unpublished).
- ²⁹M. Radparvar and J. E. Nordman, *IEEE Trans. Mag.* **MAG-21**, 888 (1985).
- ³⁰L. J. Campbell (unpublished).
- ³¹T. Aomine, *J. Low Temp. Phys.* **74**, 263 (1989).
- ³²J. Rhyner and G. Blatter, *Phys. Rev. B* **40**, 829 (1989).
- ³³J. Mannhart and C. C. Tseui (unpublished).
- ³⁴N.-C. Yeh, A. G. Schrott, and A. Gupta (private communication).
- ³⁵S. Jin, T. H. Tiefel, R. C. Sherwook, R. B. van Dover, M. E. Davis, G. W. Kammlott, and R. A. Fastnacht, *Phys. Rev. B* **37**, 7850 (1988).
- ³⁶D. R. Clarke, T. M. Shaw, and D. Dimos, *J. Am. Ceram. Soc.* **72**, 1103 (1989).
- ³⁷K. Togano, H. Kumakura, and D. R. Dietderich, *Cryogenics* **29**, 286 (1989).
- ³⁸G. R. Wagner, J. Talvacchio, and A. J. Panson, *Mater. Lett.* **6**, 390 (1988).
- ³⁹H. K pfer, S. M. Green, C. Jiang, Yu Mei, H. L. Luo, R. Meier-Hirmer, and C. Politis, *Z. Phys. B* **71**, 63 (1988).
- ⁴⁰M. Matsuda, Y. Iwai, M. Takata, M. Ishii, T. Yamashita, and H. Koinuma, *Jpn. J. Appl. Phys.* **27**, L1650 (1988).
- ⁴¹J. R. Thompson, J. Brynestad, D. M. Kroeger, Y. C. Kim, S. T. Sekula, D. K. Christen, and E. D. Specht, *Phys. Rev. B* **39**, 6652 (1989).
- ⁴²H. Kumakura, K. Togano, K. Takahashi, E. Yanagisawa, M. Nakao, and H. Maeda, *Jpn. J. Appl. Phys.* **27**, L2059 (1988).
- ⁴³H. Kumakura, K. Togano, H. Maeda, E. Yanagisawa, T. Morimoto, *Jpn. J. Appl. Phys.* **28**, L176 (1989).
- ⁴⁴O. Fischer, *Appl. Phys.* **16**, 1 (1978).
- ⁴⁵C. Rossel and O. Fischer, *J. Phys. F* **14**, 455 (1984).
- ⁴⁶Y. Hidaka and M. Suzuki, *Nature* **338**, 635 (1989).

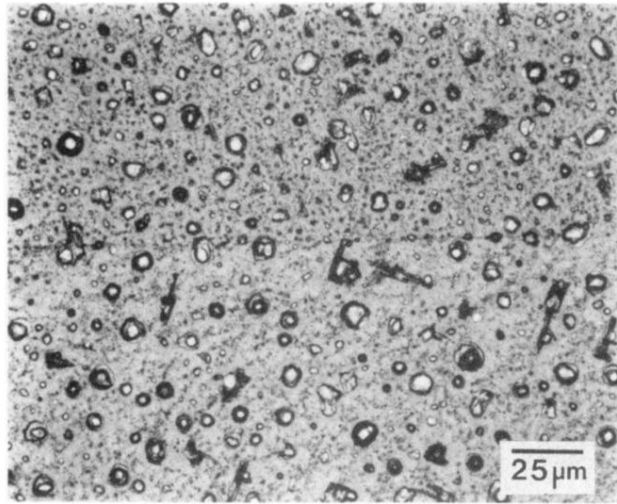


FIG. 1. Optical micrograph of the surface of a bicrystal film produced by evaporation and postannealing. The grain boundary runs through the center. Surface precipitates of CuO and small *c*-axis in-plane domains are visible. In this case, $\theta=40^\circ$, as measured by x-ray diffraction.